Separation and Purification Technology xxx (xxxx) xxx–xxx

Contents lists available at ScienceDirect

Separation and Purification Technology

journal homepage: www.elsevier.com/locate/seppur

Cost-effective synthesis of activated carbons with high surface areas for electrodes of non-aqueous electric double layer capacitors

Takeshi Mori[a], Shinichiroh Iwamura[b], Isao Ogino[b], Shin R. Mukai[b,*]

[a] Industrial Research Institute, Hokkaido Research Organization, N19W11 Kita-ku, Sapporo, Hokkaido 060-0819, Japan
[b] Division of Applied Chemistry, Graduate School of Engineering, Hokkaido University, N13W8 Kita-ku, Sapporo, Hokkaido 060-8628, Japan

ARTICLE INFO

Keywords:
Phenolic resin
Hard template
Activated carbon
Physical activation
Electric double layer capacitor

ABSTRACT

Activated carbons for electrodes of non-aqueous electric double layer capacitors were prepared from composites of poly(methymethacrylate) particles and phenolic resins. Their surface areas can be increased up to 3000 $m^2 g^{-1}$ through simple CO_2 activation. Through the characterization of pore properties of the resulting carbons, it was found that the activation process appears to be composed of two steps. The pore properties of the activated carbons were optimized to maximize their performances as electrodes for non-aqueous electric double layer capacitor electrodes.

1. Introduction

Electric double layer capacitors (EDLCs) are devices that can store energy through the adsorption and desorption of electrolyte ions on the surface of polarized electrodes [1]. Because the adsorption-desorption of electrolyte ions occurs without chemical reactions, EDLCs can charge and discharge energy at high current densities, leading to power densities higher than those of typical secondary batteries [2]. However, their energy densities are much lower than those of secondary batteries [2]. Using non-aqueous electrolytes is one of the solutions to improve the energy density of EDLCs because they have wider potential windows (1.5–3.0 V) than those of aqueous electrolytes (< 1.2 V) [3].

Carbons are often used as electrode materials of EDLCs because they have both high specific surface areas (SSAs) and electrical conductivities [4]. So far, it is reported that ordered mesoporous carbons [5,6], carbide-derived carbons [7,8] and templated carbons [9,10] exhibit high capacitances even at extremely high current densities. However, commercial EDLCs generally use carbons prepared from readily available precursors such as sawdust [11], petroleum pitches [12,13] and coconut shells [14]. Especially, KOH-activated carbons from petroleum pitches, which are known as “super activated carbons,” have extremely high SSAs as high as 3000 $m^2 g^{-1}$ [13]. The production cost of KOH-carbons are several times higher than that of carbons prepared by other methods, mainly because it requires an additional washing process to remove alkaline metal residues from the final products.

Activated carbons can be prepared cost-effectively through gas activation, where precursor carbons are gasified with oxidative gases such as steam and carbon dioxide. However, the SSAs of the activated carbons obtained through such processes are generally insufficient to be used as electrode materials. This is because the oxidative gas molecules also gasify carbons close to external surfaces without developing significant volumes of micropores. In our previous work, we succeeded in preparing carbon xerogels with SSAs as high as 3000 $m^2 g^{-1}$ by gas activation [15]. Such high SSAs can be achieved because carbon xerogels have a network of mesopores that facilitates mass transfer of the oxidative gas molecules and gasification occurs uniformly throughout the precursor carbons. However, the preparation cost of such xerogels is still high, because it requires multiple steps to introduce a network of mesopores to the resulting carbons.

Here, we propose a cost-effective method to prepare activated carbons with extremely high SSAs. Phenolic resin, which is cost-effective and a typical precursor of carbons, and which can be readily prepared through the polycondensation of phenol with formaldehyde, was used as the carbon precursor. Generally, the SSAs of carbons derived from phenolic resins can be increased only up to limited values through gas activation [16], since carbons derived from phenolic resins are essentially non-porous. Therefore, in this work, poly(methymethacrylate) (PMMA) was used as a template to introduce a network of pores to the carbons derived from phenolic resins prior to activation. PMMA is a suitable template because it decomposes at a relatively low temperature so that the template can be removed during the carbonization of the phenolic resin. Also, PMMA decomposes hardly leaving any residues [17].

Here, we report a cost-effective method to produce activated carbons with high SSAs through simple gas activation. We show that a

* Corresponding author.
E-mail address: smukai@eng.hokudai.ac.jp (S.R. Mukai).

https://doi.org/10.1016/j.seppur.2018.04.022
Received 27 December 2017; Received in revised form 6 March 2018; Accepted 6 April 2018

network of pores can readily be introduced into phenolic resin-derived carbons using PMMA particles as the template. The changes of the pore properties of the PMMA templated carbons during gas activation were analyzed. Also, the obtained carbons with various pore systems were tested as electrode materials for non-aqueous EDLCs to clarify the optimal pore properties for this application.

2. Experimental methods

2.1. Materials

Phenol (C_6H_5OH, 99.0 + %), formaldehyde solution (CH_2O, 36.0–38.0%) and sodium carbonate (Na_2CO_3, 99.8%) were purchased from Wako Pure Chemical Industries. An electrolyte solution of tetraethylammonium tetrafluoroborate ($(C_2H_5)_4NBF_4$, 1.0 mol L^{-1}) was purchased from Kishida Chemical Industries Co., Ltd. Poly(methylmethacrylate) (PMMA) particles (Chemisnow®) were kindly provided by Soken Chemical & Engineering Co., Ltd. All materials were used as received.

2.2. Synthesis of PMMA templated carbons

4.70 g of phenol (P), 105.99 mg of sodium carbonate (C), 8.11 g of formaldehyde (F) solution and 10 g of PMMA particles (1.5 μm, 0.07 μm in diameter D_p) were mixed into 24.93 g of distilled water. The obtained slurry was poured into polypropylene (PP) tubes then centrifuged at 3500 rpm. After the supernatant was removed from the PP tubes, the sediments were cured first at 333 K for 24 h then at 363 K for 48 h. The cured sediments were carbonized at 1273 K for 4 h under a flow of N_2 (100 cm^3 min^{-1}) in a tubular furnace.

2.3. Physical activation of PMMA templated carbons by CO_2 gas

The carbons were first heated to 1273 K in a flow of N_2 (100 cm^3 min^{-1}) in a tubular furnace. Once the temperature reached 1273 K, a flow of CO_2 (20 cm^3 min^{-1}) was additionally fed to the furnace to activate the carbons. The degree of activation was evaluated by calculating burn-off values, x, using Eq. (1), where m_0 and m_f denote the masses of the carbons before and after CO_2 activation, respectively. The samples will be denoted as PFR-D_p–x.

$$x = 1 - \frac{m_f}{m_0} \tag{1}$$

2.4. Characterization of the PMMA templated carbons

The morphology of the prepared materials was characterized using a field emission scanning electron microscope (FE-SEM, JEOL Ltd., JSM-6600F). Pore properties of the prepared materials were characterized through N_2 adsorption experiments conducted at 77 K using an adsorption apparatus (BELSORP-mini, Microtrac BEL). Prior to measurements, the samples were heated at 523 K for 4 h under a flow of N_2 (20 cm^3 min^{-1}). Specific surface areas S_α [m^2 g^{-1}] were calculated by applying the α_s method to the N_2 adsorption isotherms [18]. Average widths of the micropores, W_{micro} [nm], were calculated using Eq. (2), where V_{micro} [cm^3 g^{-1}] and S_{micro} [m^2 g^{-1}] denotes the pore volumes and SSAs of micropores calculated from the α_s method. The calculations were conducted under the assumption that the micropores have a slit-shape [19].

$$W_{micro} = \frac{2V_{micro}}{S_{micro}} \tag{2}$$

2.5. Electrochemical performances of the activated PMMA templated carbons

The prepared carbons were mixed with poly(tetrafluoroethylene) (PTFE) as a binder and carbon black (CB) as a conductive agent. The mass ratio of the prepared carbon, PTFE and CB was 8:1:1. The mixture was casted into a sheet with a thickness of 0.5 mm then 12 mm diameter disks were punched out from the sheet. The electrodes were degassed at 393 K for 24 h. The following steps were conducted in a glove box filled with Ar. The electrodes were placed in vials filled with a 1.0 mol L^{-1} $(C_2H_5)_4NBF_4$/PC electrolyte solution. Two-electrode type Swagelok® cells were fabricated with the prepared electrodes, current collectors and separators as shown in a previous report [15]. Galvanostatic charge-discharge tests of the cells were conducted using a charge-discharge unit (HJ-210B, Hokuto Denko Co.). The cells were charged and discharged in the potential range of 0–1.5 V at current densities set in the range of 50–1000 mA g^{-1}. Gravimetric capacitances C_g and areal capacitances C_s were calculated using Eqs. (3) and (4), respectively. $\Delta V/\Delta t$ and i denote slope of the discharging curves and current density.

$$C_g = \frac{4i}{-\Delta V/\Delta t} \tag{3}$$

$$C_s = 100 \times \frac{C_g}{S_\alpha} \tag{4}$$

3. Results and discussion

3.1. Pore properties of the PMMA templated carbons prior to activation by CO_2

Prior to activation by CO_2 gas, the pore properties of the carbons before activation were characterized by analyzing the FE-SEM images and the isotherms obtained by N_2 adsorption experiments. Fig. 1 shows

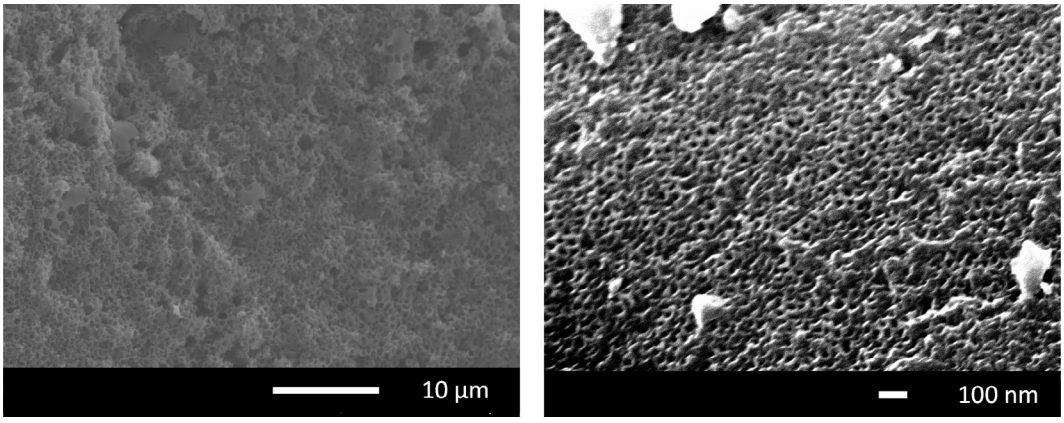

Fig. 1. FE-SEM images of PMMA templated carbons prior to CO_2 activation: (left) PFR-1.5 μm and (right) PFR-0.07 μm.

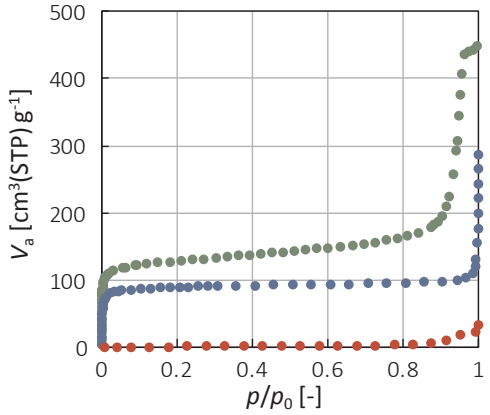

Fig. 2. Nitrogen adsorption isotherms of carbons derived from phenolic resin and PMMA templated carbons prior to CO_2 activation: (ref) PFR; (blue) PFR-1.5 μm and (green) PFR-0.07 μm.

the FE-SEM images of PFR-1.5 μm and PFR-0.07 μm. It is confirmed that spherical pores are introduced into both samples. The sizes of the pores of PFR-1.5 μm appears to be in the range of several hundreds of nanometers to several micrometers. The average diameter of the pores, D_p, was calculated to be 550 nm. When the diameter of the PMMA particles, D_{PMMA}, was decreased to 70 nm, D_p also decreased to several tens of nanometers.

The N_2 adsorption isotherms of PFR, PFR-1.5 μm and PFR-0.07 μm are shown in Fig. 2. The data for PFR did not show N_2 uptake, indicating that the pore volumes of micro- and mesopores of PFR were almost zero. On the other hand, the data for PFR-1.5 μm showed abrupt increase of N_2 uptake at an extremely high relative pressure ($p/p_0 > 0.99$). This isotherm can be classified to the type II isotherm according to the IUPAC classification [20], indicating that PFR-1.5 μm is macroporous. This result supports the results obtained from the observation of the FE-SEM image. The data for PFR-0.07 μm also showed N_2 uptake at a high relative pressure range (p/p_0 = 0.9–0.95). This isotherm can be classified as a type IV isotherm, indicating that PFR-0.07 μm is mesoporous. D_p of PFR-0.07 μm was calculated to be 40 nm by applying the Dollimore-Heal (DH) method to the isotherm.

It is confirmed that macro- or mesopores can be successfully introduced into the carbons derived from the phenolic resins. Also, the size of the pores can be tailored from several tens to hundreds of nanometers by changing the size of the PMMA particles.

3.2. Pore properties of the PMMA templated carbons activated by CO_2 gas

The pore properties of the PMMA templated carbons activated by CO_2 gas were characterized through N_2 adsorption experiments to investigate how micropores of the carbons develop during activation. The volumes of micropores V_{micro}, the specific surface areas (SSAs) S_α and the average widths of micropores W_{micro} were calculated by analyzing the N_2 isotherms of PFR, PFR-1.5 μm and PFR-0.07 μm with various burn-off values, x. The pore properties of the samples are summarized in Table 1.

Fig. 3(A-1) shows the change of V_{micro} of PFR with respect to x. When x is increased to 0.73, V_{micro} also increased from 0 $cm^3 g^{-1}$ to 0.55 $cm^3 g^{-1}$. This value is equivalent to a S_α of 1470 $m^2 g^{-1}$, which is a value close to the SSAs of typical activated carbons produced by physical activation [16]. Fig. 3(A-2) shows the change of V_{micro} of PFR-1.5 μm. V_{micro} monotonously increased from 0.14 $cm^3 g^{-1}$ to 0.59 $cm^3 g^{-1}$ with the increase in x, when x is in the range of 0–0.44. However, further increase of x up to 0.91 did not result in a large increase in V_{micro} (V_{micro} of PFR-1.5 μm-0.91 was 1.00 $cm^3 g^{-1}$). S_α of PFR-1.5 μm-0.91 was 2170 $m^2 g^{-1}$, which is equivalent to the values of typical activated carbon fibers [21]. In the case of PFR-0.07 μm, V_{micro} changes similarly as the PFR-1.5 μm series. When x is increased to 0.53, V_{micro} also linearly increased with x and finally reached 1.01 $cm^3 g^{-1}$. V_{micro} only increased up to 1.11 $cm^3 g^{-1}$ when x was further increased to 0.80. S_α of PFR-0.07 μm-0.53 was 3010 $m^2 g^{-1}$, which exceeds the SSA of typical alkali-activated carbons (MSC-30, 2710 $m^2 g^{-1}$) and is equivalent to activated carbon aerogels (< 3000 $m^2 g^{-1}$) [16,22]. For both PFR-1.5 μm and PFR-0.07 μm, there appears to be a threshold between the region where V_{micro} significantly increases with x (region I, x = 0–0.44 in the case of PFR-1.5 μm, x = 0–0.53 in the case of PFR-0.07 μm) and the region where V_{micro} only slightly increases (region II, $x > 0.44$ in the case of PFR-1.5 μm, $x > 0.53$ in the case of PFR-0.07 μm). Fig. 3(B) shows how W_{micro} of CO_2-activated PFR, PFR-1.5 μm and PFR-0.07 μm, changes with respect to x. Without activation, PFR-1.5 μm and PFR-0.07 μm have almost the same W_{micro} (0.70 nm, 0.68 nm, respectively). In the case of PFR-1.5 μm-0.28, W_{micro} was 0.69 nm, which is almost the same value as that of PFR-1.5 μm (0.70 nm). However, when x is increased to values larger than 0.28, W_{micro} linearly increased with x and reached 0.93 nm (x = 0.91). A similar change in W_{micro} was observed for PFR-0.07 μm. W_{micro} of PFR-0.07 μm-0.21 and PFR-0.07 μm-0.37 were respectively 0.66 nm and 0.69 nm, which values are also similar to that of PFR-0.07 μm (0.68 nm). Meanwhile, W_{micro} of PFR-0.07 μm-0.80 was 0.79 nm, which is slightly larger than that of PFR-0.07 μm at a lower x. There also appears to be a threshold between the region where W_{micro} remains constant (x = 0–0.28 in the case of PFR-1.5 μm, x = 0–0.37 in the case of PFR-0.07 μm) and the region where W_{micro} increases with x (region II, $x > 0.28$ in the case of PFR-1.5 μm, $x > 0.37$ in the case of PFR-0.07 μm). These two regions almost correspond to region I and the region II, respectively.

Based on the trends in the changes of V_{micro} and W_{micro}, it seems that CO_2 activation of PFR-1.5 μm and PFR-0.07 μm proceeds through two steps as shown in Fig. 4 and Table 2, which is quite similar as in the case of the activation of carbon aerogels by CO_2 gas [15]. In the first step, where x is relatively small (x is less than approximately 0.3–0.4 (PFR-1.5 μm) or 0.4–0.5 (PFR-0.07 μm)), V_{micro} increases with x and W_{micro} remains the same as that of the precursor carbon. In this step, the activating reagent, CO_2, is thought to gasify carbon to "lengthen" the micropores, resulting in an effective increase in SSA. On the other hand, in the next step, where x is greater than the threshold value (x is greater than 0.3–0.4 (PFR-1.5 μm) or 0.4–0.5 (PFR-0.07 μm)), V_{micro} slightly increases and W_{micro} increases with x. In this step, carbon is considered

Table 1
Textural properties of PMMA templated carbons and activated PMMA templated carbons.

Sample	S_α [$m^2 g^{-1}$][a]	V_{micro} [$cm^3 g^{-1}$][b]	W_{micro} [nm][c]	$C_{g,50}$ [$F g^{-1}$][d]
PFR	10	0.00	0.57	–
PFR-0.73	1470	0.55	0.79	55.9
PFR-1.5 μm	410	0.14	0.70	–
PFR-1.5 μm-0.28	1190	0.41	0.69	–
PFR-1.5 μm-0.44	1570	0.59	0.76	71.6
PFR-1.5 μm-0.91	2170	1.00	0.93	–
PFR-0.07 μm	570	0.16	0.68	–
PFR-0.07 μm-0.21	1680	0.49	0.66	66.4
PFR-0.07 μm-0.37	1900	0.60	0.69	77.7
PFR-0.07 μm-0.53	3010	1.01	0.75	84.5
PFR-0.07 μm-0.80	3270	1.11	0.79	–

[a] Specific surface area, S_α, calculated by the α_s method.
[b] Micropore volume V_{micro} calculated by the α_s method.
[c] Average width of micropore, W_{micro} calculated using Eq. (2).
[d] Gravimetric capacitance $C_{g,\ 50}$ calculated from the discharging curves measured at 50 mA g^{-1}.

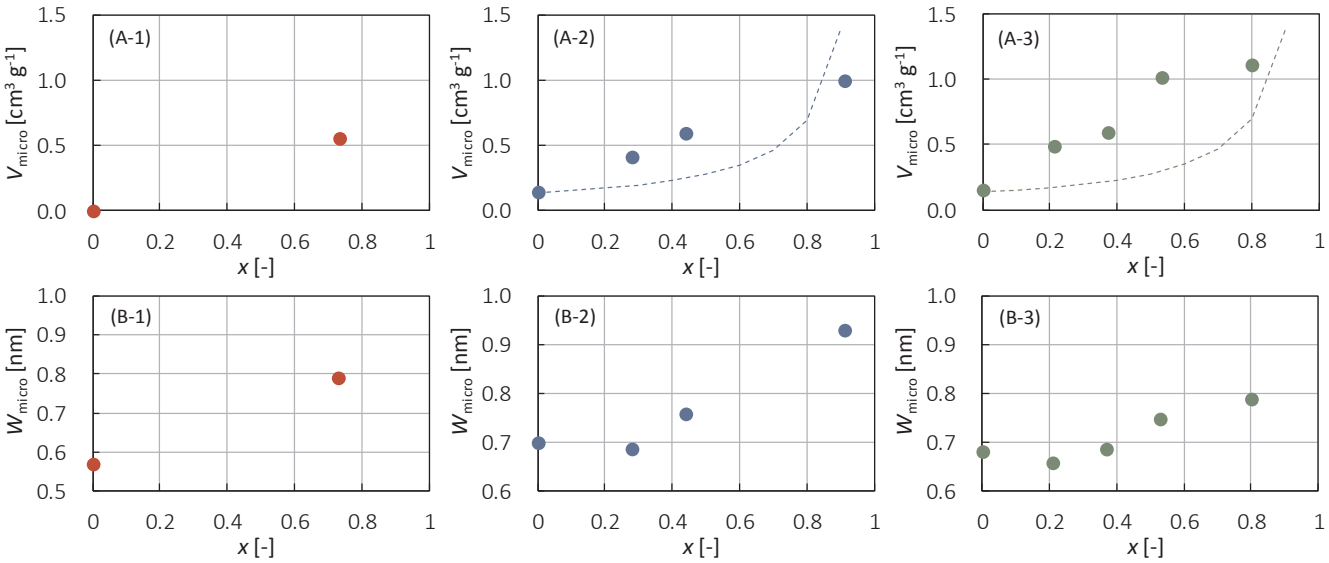

Fig. 3. (A) Change of pore volumes of micropores and (B) average widths of the micropores of the prepared PMMA templated carbons: (A-1) and (B-1) PFR series; (A-2) and (B-2) PFR-1.5 μm series; (A-3) and (B-3) PFR-0.07 μm series. The dashed lines are the hypothetical volumes of micropores V_{micro}'.

to be gasified in the following two manners: (i) CO_2 gasifies carbon to "widen" the structure of the micropores and (ii) carbon located on the external surfaces are gasified without micropore development. Activation proceeds less efficiently in terms of specific surface area.

Since the aim of this work is to produce activated carbons with high SSAs, it is thought that the precursor carbon must be activated to high degrees. In such cases, the increase of SSA is mainly caused by the decrease in weight due to carbon consumption, rather than the development of micropores. For example, when a carbon precursor with an SSA of 500 $m^2 g^{-1}$ is gasified without the development or loss of any nanopores (the absolute value of surface area [m^2] remains constant) to a burn-off value of 80%, the SSA of the resulting carbon becomes 2500 $m^2 g^{-1}$. Here, we define a hypothetical volume of micropores V_{micro}'. V_{micro}' is the micropore volume of activated carbons prepared through an imaginary process where its precursor carbon is gasified without any development of micropores. V_{micro}' can be calculated using Eq. (5), where $V_{micro,\ 0}$ denotes the micropore volume of the precursor carbon ($x = 0$). By comparing V_{micro} (calculated from N_2 adsorption experiments) and V_{micro}', it can be estimated whether the increase in SSA of the activated carbon is simply caused by weight reduction, or if there are any contribution of pore development to the increase in SSA.

Table 2
Changes of pore properties of the activated carbons during CO_2 activation.

	Region I	Region II
V_{micro}	Increases	Slightly increases
W_{micro}	Remains constant	Increases
How CO_2	"lengthening" of the micropores	"widening" of the micropores
Gasifies carbons		Gasifying carbons on external surfaces

$$V'_{micro} = \frac{V_{micro,0}}{1-x} \quad (5)$$

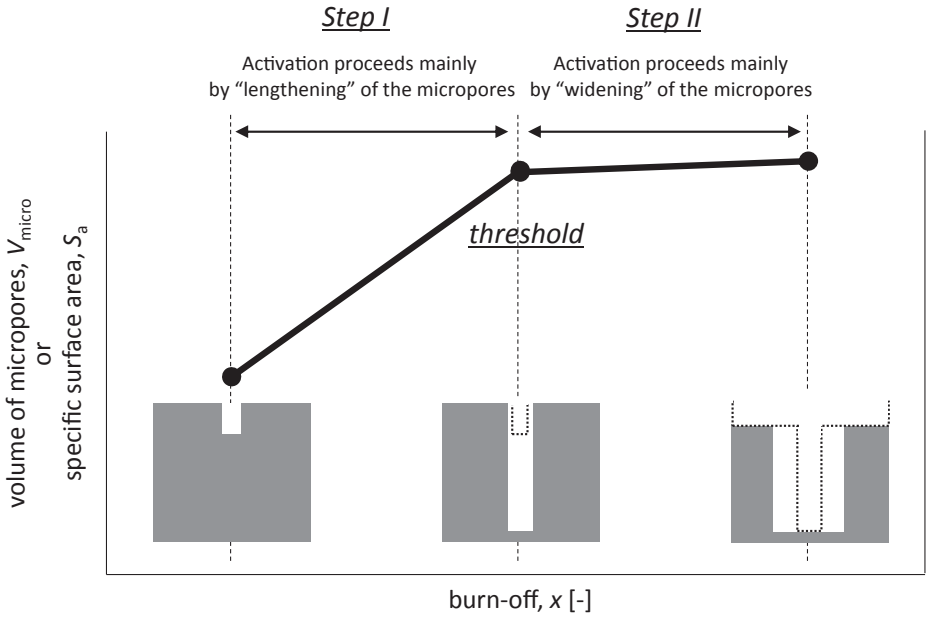

Fig. 4. Illustration of the structural change of micropores developed in PMMA templated carbons during the CO_2 activation.

The dashed lines in Fig. 3(A) show the changes of V_{micro}' with respect to x. If V_{micro} is over the dashed line, the increase in V_{micro} can be attributed to the increase in the absolute volume of micropores. As for the PFR-1.5 μm series, V_{micro} of PFR-1.5 μm-0.28 and PFR-1.5 μm-0.44 were over the dashed line, whereas V_{micro} of PFR-1.5 μm-0.91 was under the dashed line. Also, V_{micro} of PFR-0.07 μm-0.21, PFR-0.07 μm-0.37 and PFR-0.07 μm-0.53 were over the dashed line, whereas V_{micro} of PFR-0.07 μm-0.80 was almost on the line. For both series, it is observed that V_{micro} is always larger than V_{micro}' at a moderate x ($x <$ approximately 0.6), indicating that the absolute volume of micropores increased. Also, there is a trend that V_{micro} is equal to or smaller than V_{micro}' at extremely high x values ($x >$ approximately 0.80), indicating that carbons are gasified without increasing the absolute volume of micropores. The difference between V_{micro} and V_{micro}' became maximum at $x = 0.44$ in the case of the PFR-1.5 μm series and at $x = 0.53$ in the case of the PFR-0.07 μm series. The most efficiently activated carbons in all the sample series studied in this work were PFR-1.5 μm-0.44 and PFR-0.07 μm-0.53. From this point of view, when preparing the activated carbons with high SSAs, extremely high activation degree should be avoided since the increase in SSA in such highly activated carbons is hardly caused by actual development of micropores.

3.3. Electrochemical performances of the PMMA templated carbons activated by CO_2 gas

The electrochemical performances of PMMA templated carbons prepared at different x values which have various D_p were characterized to optimize the pore properties of the carbon for non-aqueous EDLC electrodes. The electrodes fabricated from the PMMA templated carbons, PTFE and CB were set in a two-electrode type cell filled with a 1.0 mol L^{-1} $(C_2H_5)_4NBF_4$/PC solution. The cell was charged and discharged at a current density set in the range of 50–1000 mA g^{-1}. Typical charging and discharging curves of samples of the PFR-0.73, PFR-1.5 μm-0.44 and PFR-0.07 μm series (PFR-0.07 μm-0.21, PFR-0.07 μm-0.37 and PFR-0.07 μm-0.53) measured at 100 mA g^{-1} are shown in Fig. 5(A), (B) and (C), respectively. It was confirmed that the potential, ΔE, almost linearly increased with time t during charging ($t < 0$) and linearly decreased during discharging ($t > 0$). This indicates that the charge-discharge processes proceed through a physical process of adsorption and desorption of electrolyte ions.

Fig. 6 shows the gravimetric capacitance measured at 50 mA g^{-1}, $C_{g,50}$, of the five samples. $C_{g,50}$ was plotted against the specific surface area of the carbons S_a to elucidate how SSA affects capacitance. $C_{g,50}$ increased with S_a and finally reached to 84.6 F g^{-1} (PFR-0.07 μm-0.53). This value is approximately 1.4–2.8 times higher than that of the typical activated carbons previously reported (30–60 F g^{-1}) [23]. $C_{g,50}$ of PFR-0.73 (S_a = 1470 m^2 g^{-1}), PFR-1.5 μm-0.44 (S_a = 1570 m^2 g^{-1}) and PFR-0.07 μm-0.21 (S_a = 1680 m^2 g^{-1}) were 55.9 F g^{-1}, 71.6 F g^{-1} and 66.4 F g^{-1}. Although the three samples have similar SSAs, their $C_{g,50}$ were significantly different. This difference of $C_{g,50}$ might be because the size of micropores, W_{micro}, are different among the three samples. Chmiola et al., reported that decreasing the average pore size of electrode materials down to sub- nanometer range, which is less than the size of the solvated TEA^+ cations, abruptly increases areal capacitance, C_s [7]. The distortion of the solvation shell of the cation occurs in sub-nanometer sized micropores, allowing the cations to approach closer to the pore walls. C_s of PFR-1.5 μm-0.44 (W_{micro} = 0.69 nm) was 4.6 μF cm^{-2}, which is higher than the value of PFR-0.73 (C_s = 3.8 μF cm^{-2}, W_{micro} = 0.79 nm). The higher $C_{g,50}$ of PFR-1.5 μm-0.44 can be attributed to the smaller width of its micropores. However, although W_{micro} of PFR-0.07 μm-0.21 (W_{micro} = 0.66 nm) was smaller than that of PFR-1.5 μm-0.44 (W_{micro} = 0.69 nm), C_s of PFR-0.07 μm-0.21 was 3.9 μF cm^{-2}. In this case, W_{micro} is smaller than the diameter of the naked TEA^+ (0.68 nm), therefore the cations are not able to be accommodated in some of the micropores in PFR-0.07 μm-0.21, resulting in the decrease in capacitance.

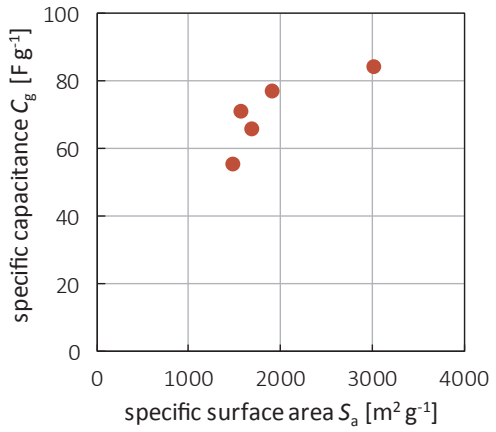

Fig. 6. Gravimetric specific capacitances of PMMA templated carbons prepared at different x values which have various D_p calculated from the discharge curves measured at 50 mA g^{-1}.

Fig. 7(A) shows C_g of PFR-0.73, PFR-1.5 μm-0.44 and PFR-0.07 μm-0.21 measured at a current density set in the range of 50–1000 mA g^{-1} to investigate how the meso-, or macropore structure of the carbon affects rate performance. At low current densities (< 200 mA g^{-1}), C_g of PFR-1.5 μm-0.44 (C_g = 64–72 F g^{-1}) and PFR-0.07 μm-0.21 (C_g = 60–66 F g^{-1}) were higher than that of PFR-0.73 (C_g = 47–56 F g^{-1}). It is considered that the rate performance can be improved by introducing meso-, or macropores even at such low current densities. However, at the highest current density (1000 mA g^{-1}),

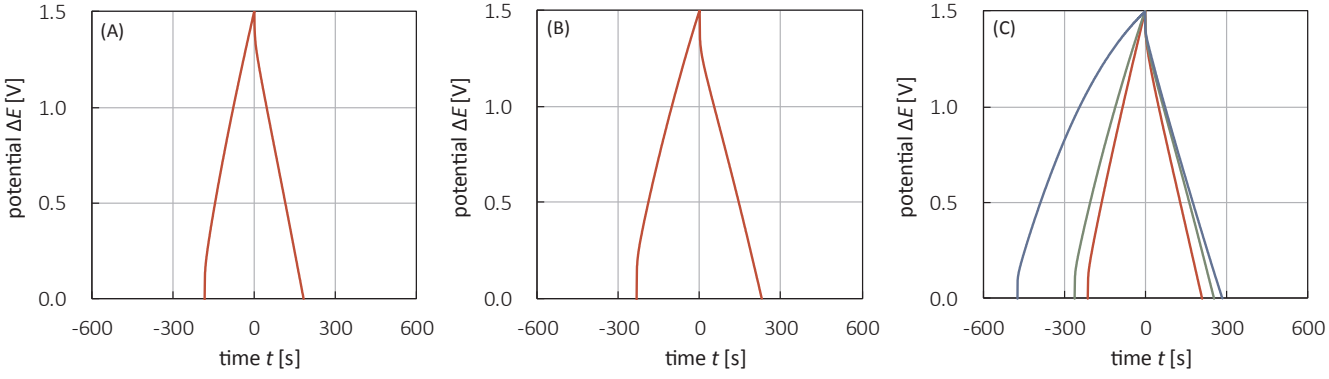

Fig. 5. Galvanostatic charge-discharge curves of the PMMA templated carbons activated by CO_2 gas: (A) PFR-0.73; (B) PFR-1.5 μm-0.44 and (C) PFR-0.07 μm series (PFR-0.07 μm-0.21 (red), PFR-0.07 μm-0.37 (green) and PFR-0.07 μm-0.53 (blue)) measured at 100 mA g^{-1}. (For interpretation of the references to colour in this figure legend, the reader is referred to the web version of this article.)

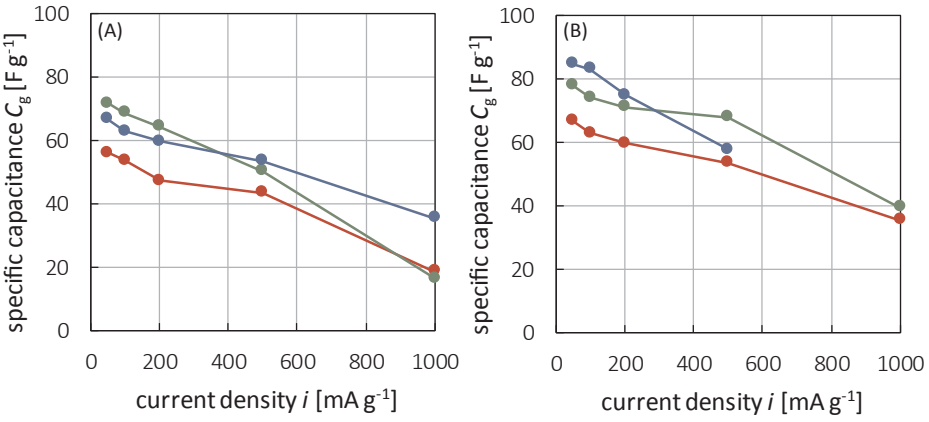

Fig. 7. Gravimetric capacitances calculated from discharging curves measured at current densities set in the range of 50–1000 mA g^{-1}: (A) PFR-0.73 (red), PFR-1.5 μm-0.44 (green) and PFR-0.07 μm-0.21 (blue); (B) PFR-0.07 μm-0.21 (red), PFR-0.07 μm-0.37 (green) and PFR-0.07 μm-0.53 (blue). (For interpretation of the references to colour in this figure legend, the reader is referred to the web version of this article.)

C_g of PFR-0.07 μm-0.21 (C_g = 35 F g^{-1}) was approximately twice than that of PFR-1.5 μm-0.44 (C_g = 16 F g^{-1}). At such a high current density, diffusion paths with sizes of several tens of nanometers should be introduced into carbons to retain its capacitance, since such diffusion paths are considered to facilitate mass transport of the electrolytes, leading to the improvement of the capacitance at high current densities [15].

Fig. 7(B) shows C_g of PFR-0.07 μm-0.21, PFR-0.07 μm-0.37 and PFR-0.07 μm-0.53 measured at a current density set in the range of 50–1000 mA g^{-1} to investigate how the degree of activation affects rate performance. At low current densities (< 200 mA g^{-1}), C_g tends to increase with the increase in x. Among the three samples, PFR-0.07 μm-0.53 exhibited the highest C_g (75–85 F g^{-1}). However, at high current densities (500 mA g^{-1}), C_g of PFR-0.07 μm-0.53 drastically decreased to 58 F g^{-1}, which is lower than that of PFR-0.07 μm-0.37 (68 F g^{-1}) and is almost the same value as that of PFR-0.07 μm-0.21 (53 F g^{-1}). When the current density was further increased to 1000 mA g^{-1}, C_g of PFR-0.07 μm-0.53 could not be calculated from its discharging curve because a large potential drop was observed at the beginning of the discharge process. On the other hand, at 1000 mA g^{-1}, potential drops of PFR-0.07 μm-0.21 and PFR-0.07 μm-0.37 were not as large as that of PFR-0.07 μm-0.53. Their C_g were calculated to be 35 F g^{-1} and 39 F g^{-1}, respectively. Electrical resistivity of PFR-0.07 μm-0.37 and PFR-0.07 μm-0.53 were estimated from the relationship between the potential drop at the beginning of discharging and current density. Electrical resistivity of PFR-0.07 μm-0.53 (7.5 Ω m^{-1}) was significantly higher than that of PFR-0.07 μm-0.37 (3.2 Ω m^{-1}). This increase in electrical resistivity with x might have caused an abrupt decrease in C_g at such high current densities.

To achieve both a high gravimetric capacitance and a good rate performance, carbons with the two following properties should be used: (i) mesopores that allows fast mass transport of electrolyte ions, (ii) an optimum volume of micropores providing moderately high SSA without severely decreasing its electrical conductivity.

4. Conclusion

Using PMMA templated carbons derived from phenolic resins, we successfully prepared activated carbons with extremely high SSAs over 3000 m^2 g^{-1} through simple CO_2 activation. By analyzing how the SSA and volume of micropores of the carbons change during activation, the introduction of a network of pores with sizes of several tens of nanometers was found to significantly improve the efficiency of activation. It was also revealed that the process of CO_2 activation can be divided into two steps. In the first step, CO_2 appears to gasify the precursor carbon to “lengthen” the micropores. In the next step, it seems that “widening” of the micropores as well as the consumption of carbons at the external surfaces occurs simultaneously. There is a threshold between the two steps, and which can easily be found by plotting micropore widths and volumes against the degree of activation. To develop micropores effectively, the target burn-off value should be set around this threshold value. The pore structures of the activated carbons were optimized to maximize its performance as electrodes for non-aqueous EDLCs. Gravimetric capacitance increased with SSA and finally reached 84.6 F g^{-1}, which is significantly higher than that of typical activated carbons.

References

[1] D. Qu, H. Shi, Studies of activated carbons used in double-layer capacitors, J. Power Sources 74 (1998) 99–107.
[2] B.D. McCloskey, Expanding the Ragone plot: pushing the limits of energy storage, J. Phys. Chem. Lett. 6 (2015) 3592–3593.
[3] H. Nishihara, T. Kyotani, Templated nanocarbons for energy storage, Adv. Mater. 24 (2012) 4473–4498.
[4] E. Frackowiak, F. Beguin, Carbon materials for the electrochemical storage of energy in capacitors, Carbon 39 (2001) 937–950.
[5] A.B. Fuertes, G. Lota, T.A. Centeno, E. Frackowiak, Templated mesoporous carbons for supercapacitor application, Electrochim. Acta 50 (2005) 2799–2805.
[6] H. Liu, W. Cui, L. Jin, C. Wang, Y. Xia, Preparation of three-dimensional ordered mesoporous carbon sphere arrays by a two-step templating route and their application for supercapacitors, J. Mater. Chem. 19 (2009) 3661–3667.
[7] J. Chmiola, G. Yushin, Y. Gogotsi, C. Portet, P. Simon, P.L. Taberna, Anomalous increase in carbon capacitance at pore sizes less than 1 nanometer, Science 313 (2006) 1760–1762.
[8] Y. Korenblit, M. Rose, E. Kockrick, L. Borchardt, A. Kvit, S. Kaskel, G. Yushin, High-rate electrochemical capacitors based on ordered mesoporous silicon carbide-derived carbon, ACS Nano 4 (2010) 1337–1344.
[9] S. Woo, K. Dokko, H. Nakano, K. Kanamura, Preparation of three dimensionally ordered macroporous carbon with mesoporous walls for electric double-layer capacitors, J. Mater. Chem. 18 (2008) 1674–1680.
[10] Y. Zhao, M. Zheng, J. Cao, X. Ke, J. Liu, Y. Chen, J. Tao, Easy synthesis of ordered meso/macroporous carbon monolith for use as electrode in electrochemical capacitors, Mater. Lett. 62 (2008) 548–551.
[11] J. Matos, C. Nahas, L. Rojas, M. Rosales, Synthesis and characterization of activated carbon from sawdust of algarroba wood. 1. Physical activation and pyrolysis, J. Hazard. Mater. 196 (2011) 360–369.
[12] Kuraray Chemical Co., Ltd, Honda Giken Kogyo Kabushiki Kaisha, Activated carbon, method for production thereof, polarized electrode and electrical double layer capacitor (2004), WO2004011371 A1.
[13] Kansai Coke & Chem Co., Ltd., Carbon Tech KK, Manufacturing Method of Activated Carbon, and Electric-double Layer Capacitor Using Activated Carbon Obtained by the Manufacturing Method, JP 2011-011935.
[14] Kuraray Chemical Co., Ltd., Active Carbon for Gas Phase Adsorption, JP2016-187794.
[15] T. Tsuchiya, T. Mori, S. Iwamura, I. Ogino, Shin R. Mukai, Binderfree synthesis of high-surface-area carbon electrodes via CO_2 activation of resorcinol-formaldehyde carbon xerogel disks: analysis of activation process, Carbon 76 (2014) 240–249.
[16] C.F. Martin, M.G. Plaza, S. Garcia, J.J. Pis, F. Rubiera, C. Pevida, Microporous phenol-formaldehyde resin-based adsorbents for pre-combustion CO_2 capture, Fuel 90 (2011) 2064–2072.
[17] M.C. Costache, D. Wang, M.J. Heidecker, E. Manias, C.A. Wilkie, The thermal degradation of poly(methyl methacrylate) nanocomposites with montmorillonite layered double hydroxides and carbon nanotube, Polym. Adv. Technol. 17 (2006) 272–280.
[18] K.S.W. Sing, The use of physisorption for the characterization of microporous carbons, Carbon 27 (1989) 5–11.
[19] K. Kaneko, Fundamentals of gas adsorption for characterization of carbon materials, Tanso 186 (1999) 50–53.
[20] M. Thommes, K. Kaneko, A.V. Neimark, J.P. Olivier, F. Rodriguez-Reinoso,

J. Rouquero, K.S.W. Sing, Physisorption of gases, with special reference to theevaluation of surface area and pore size distribution (IUPAC technical report), Pure Appl. Chem. 87 (2015) 1051–1069.

[21] M.J. Sanchez-Montero, F. Salvador, C. Izquierdo, Reactivity and porosity of a carbon fiber activated with supercritical CO_2, J. Phys. Chem. C 112 (2008) 4991–4999.

[22] Y. Hanzawa, K. Kaneko, Activated carbon aerogels, Langmuir 12 (1996) 6167–6169.

[23] M. Inagaki, H. Konno, O. Tanaike, Carbon materials for electrochemical capacitors, J. Power Sources 195 (2010) 7880–7903.